

DOI: 10.1002/chem.201102502

Gold(I) Styrylbenzene, Distyrylbenzene, and Distyrylnaphthalene Complexes: High Emission Quantum Yields at Room Temperature

Lei Gao,^[a] Daniel S. Niedzwiecki,^[a] Nihal Deligonul,^[a] Matthias Zeller,^[b]
Allen D. Hunter,^[b] and Thomas G. Gray*^[a]

Abstract: One gold(I)-substituted styrylbenzene, six digold(I) distyrylbenzenes, one tetragold distyrylbenzene, and four digold distyrylnaphthalene complexes were synthesized using base-promoted auration, alkynylation, triazolite formation, and Horner–Wadsworth–Emmons reactions. The gold(I) fragments are either σ -bonded to the aromatic system, or they are attached through an alkynyl or triazolite spacer. Product formation was moni-

tored using $^{31}\text{P}\{^1\text{H}\}$ NMR spectroscopy. Systems in which gold(I) binds to the central benzene ring or the terminal phenyl rings were designed. All of these complexes have strong ultraviolet absorptions and emit blue light. The

position of the gold(I) attachment influences the luminescence efficiency. Complexes with two gold(I) fragments attached to the ends of the conjugated system have fluorescence quantum yields up to 0.94, when using 7-diethylamino-4-methylcoumarin as the emission standard. Density-functional theory calculations on three high-yielding emitters suggest that luminescence originates from the distyrylbenzene or -naphthalene bridge.

Keywords: alkynyl complexes • density functional calculations • gold • luminescence • phosphine ligands • quantum yields

Introduction

Distyrylbenzenes and -naphthalenes are widely studied for their versatile electroluminescence and photoluminescence.^[1] They have applications in light-emitting diodes,^[2,3] as oxygen sensitizers,^[4] nonlinear optical (NLO) materials,^[5,6] organic field effect transistors (OFETs),^[7] and as building blocks for polymers in emission sensors and solar cells.^[8] The electronic and luminescence properties of these molecules can be altered by changing the conjugation length or with electron-donating or -withdrawing substituents.^[9–16] By placing substituents along oligophenylenevinylene (OPV) or oligophenyleneethynylene (OPE) rims, chromophores with large two-photon absorption cross sections have been prepared.^[4] OPVs bearing water-solubilizing substituents have been proposed for photodynamic therapy.^[17] Recent work has linked hole-conducting OPVs to electron-conducting fullerenes to generate high-efficiency photovoltaic materials.^[18–20] In designing the active layers of light-emitting diodes, triple bonds were introduced to poly(pheny-

lene vinylene)s (PPVs) to enhance their electron affinities, thus increasing the electroluminescence efficiencies.^[21–23] A new class of 2D, π -conjugated, skewed H-shaped, co-oligomers of phenylene vinylene (PV) and phenylene ethynylene (PE) has been synthesized.^[24] These co-oligomers, which have pendant amino groups, show high fluorescence sensitivity to Brønsted acids and transition-metal ions. Yamaguchi, Jäkle, and their respective co-workers have shown that introducing boryl substituents to OPVs^[25–27] yields emissive materials with quantum yields up to 0.99.^[28] The emission yields are attributed to p_π - π^* conjugation between the vacant p orbital on boron and π orbitals of the conjugated framework. It also has been shown that attaching boryl substituents at the end positions of the π -conjugated framework or to the central core leads to different properties.

Research in this laboratory has developed the selective auration of carbon skeletons to explore the photophysical consequences of gold attachment.^[29–35] Phosphine–gold(I) fragments are isolobal with a proton.^[36] They are soft Lewis acids that activate soft electrophiles, such as π systems.^[37] The spin-orbit coupling constant of 5d electrons in gold is 5090 cm^{-1} .^[38] Its heavy atom effect ($Z=79$) influences both ground- and excited-state properties. Gold(I) is typically linear, with a coordination number of two.^[39] When bonded to aromatic rings, the spin-orbit coupling of gold allows access to triplet excited states. Strong triplet-state emission can be observed at room temperature.^[29–31,35]

Two-coordinate gold(I) is a fourteen-electron fragment with an empty 6p orbital of π symmetry. As with boryl-substituted compounds, the possibility of p - π conjugation between gold(I) and aromatic carbon invites photophysical study, here for metalated OPVs and OPEs. Most research

[a] Dr. L. Gao, D. S. Niedzwiecki, N. Deligonul, Prof. T. G. Gray
Department of Chemistry
Case Western Reserve University
10900 Euclid Avenue, Cleveland, Ohio 44106 (USA)
Fax: (+1) 216-368-3006
E-mail: tgray@case.edu

[b] M. Zeller, A. D. Hunter
Department of Chemistry
Youngstown State University
One University Plaza, Youngstown, Ohio 44555 (USA)

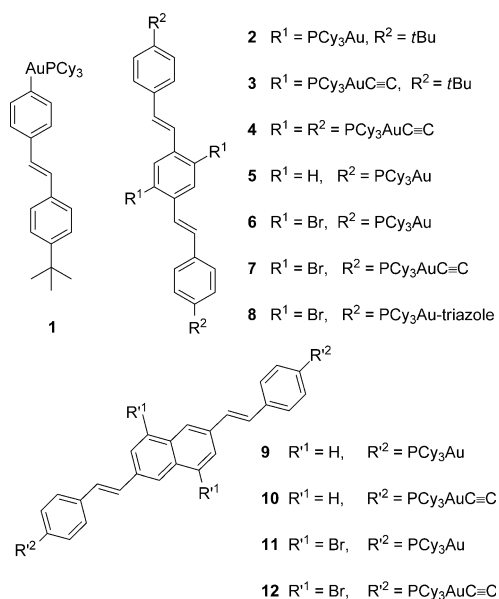
Supporting information for this article is available on the WWW under <http://dx.doi.org/10.1002/chem.201102502>.

efforts focus on modifying chromophores with conventional substituents, such as alkyls, amino groups, and halides.^[40] Studies on the effects of metal substitution have been limited.

Here we report the synthesis and optical spectroscopy of new gold(I)-substituted styrylbenzenes, distyrylbenzenes (DSBs), and distyrylnaphthalenes (DSNs). Cy_3PAu^+ fragments were attached to the DSB and DSN systems to probe the effect of gold on the photophysical properties of the hydrocarbon skeleton. Some twelve new compounds, including one mono-, ten di-, and one tetragold compound, were prepared and characterized. Their optical spectra were collected, and the fluorescence quantum yields were measured. The new compounds have blue emissions, and the most emissive are those with two Cy_3PAu^+ fragments attached to the ends of the π -conjugated systems. All compounds show strong singlet-state emissions, and no triplet emission was observed at room temperature. Crystal structures were collected for the mono- and tetragold compounds; the gold(I) centers are linear. The electronic structures of representative compounds have been examined with density-functional theory calculations.

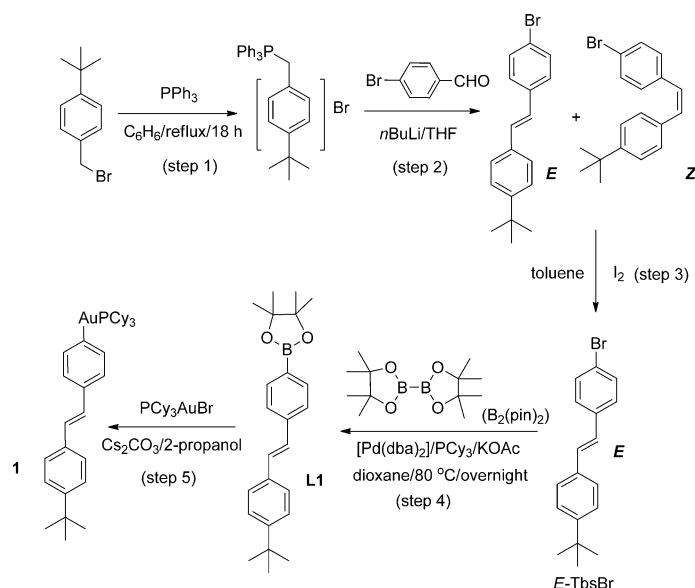
Results and Discussion

Scheme 1 sets out the new organogold compounds. These include one monogold(I) complex (**1**), ten digold complexes (**2**, **3**, **5–12**) and one tetragold complex (**4**). In complexes **1**, **2**, **5**, **6**, **9** and **11**, the Cy_3PAu fragment is σ -bonded to the aromatic ring. In compounds **3**, **4**, **7**, **10** and **12**, a $\text{C}\equiv\text{C}$ bond is installed between the aromatic ring and the Cy_3PAu fragment. In compound **8**, the Cy_3PAu fragment is attached to the 4-carbon on a triazole ring, which is connected to the aromatic ring at the 5-position.



Scheme 1.

Syntheses: Scheme 2 shows the synthetic pathway leading to **1**. Five steps are involved. A phosphonium bromide precursor was synthesized by refluxing a benzene solution of tri-

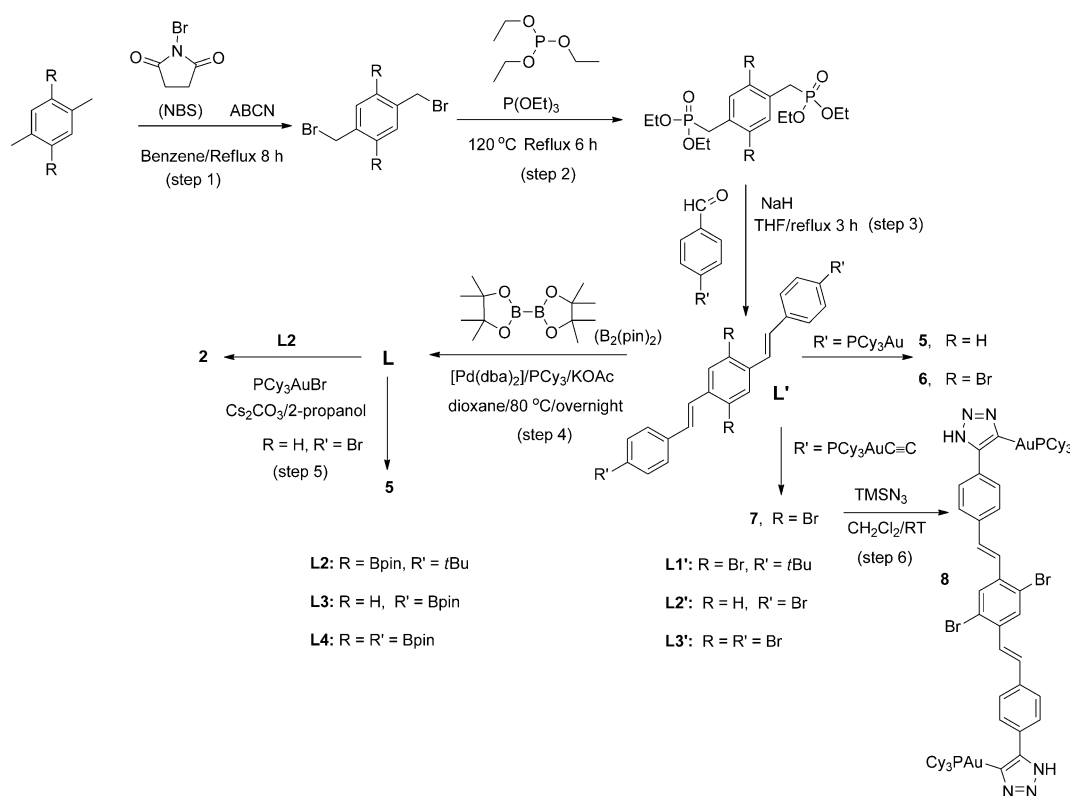


Scheme 2. Synthesis of **1**.

phenylphosphine and 4-*tert*-butylbenzyl bromide (Scheme 2 step 1). The phosphonium bromide salt was then dissolved in THF and cooled to -78°C . *n*BuLi was added slowly to this solution, which took on a tan color. A solution of 4-bromobenzaldehyde in THF was then added, and the resulting mixture was stirred overnight (Scheme 2, step 2). After the completion of the reaction, 2-propanol was used to quench excess *n*BuLi. An orange residue was collected by evaporation. Adding ethanol to this orange residue led to the isolation of a white iridescent product. This product is a mixture of both the *E* and *Z* isomers of 1-(4-bromostyryl)-4-*tert*-butylbenzene (TbsBr). Converting all the products into the *E* isomer is achieved by refluxing them in toluene with an I_2 crystal (Scheme 2, step 3).

The palladium-catalyzed cross coupling of bis(pinacolato)diboron^[41] with the (*E*)-TbsBr was then carried out to make **L1** (Scheme 2, step 4), which was purified by vacuum sublimation. Subsequent base-promoted auration^[30,35] afforded **1** (Scheme 2, step 5), which was isolated as a white powder.

Scheme 3 shows syntheses of compounds **2** and **5–8**. There are five steps in the synthesis of each. The commercially available 1,4-dimethylbenzene with or without two Br substituents first underwent bromination with *N*-bromosuccinimide in benzene under reflux with a chain initiator, 1,1'-azobis(cyclohexanecarbonitrile) (ABCN; Scheme 3, step 1). The isolated products were then combined with triethyl phosphite and refluxed for 6 h (Scheme 3, step 2), in a Michaelis–Arbuzov reaction,^[42] to yield phosphonates. Upon cooling, the phosphonates precipitated out, and were collected by filtration. Additional products could be recovered upon the addition of hexanes. After the phosphonates were



Scheme 3. Syntheses of **2** and **5–8**.

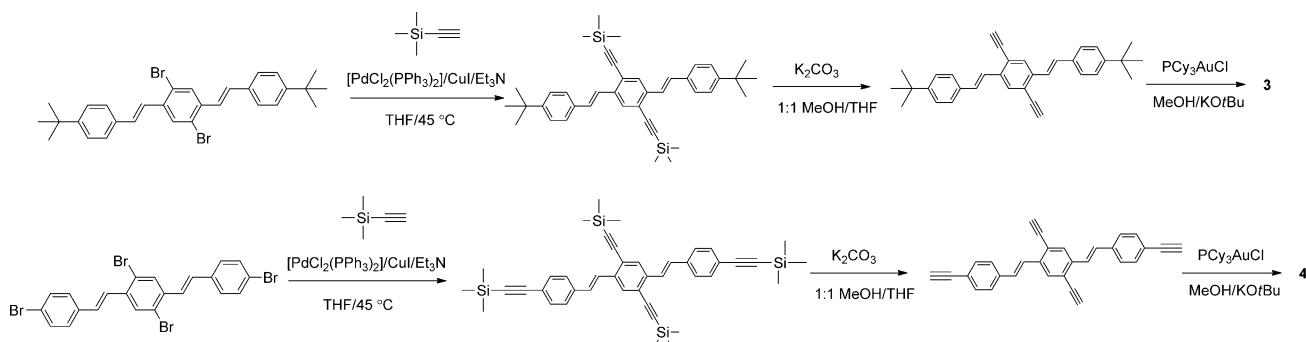
collected, Horner–Wadsworth–Emmons reactions were then carried out to produce the distyryl benzene skeletons, **L'** (Scheme 3, step 3). Products were isolated by adding water to the suspension in THF, and collected by filtration. Compounds **5**, **6**, and **7** were directly synthesized in this step with 4-(Cy₃PAu)benzaldehyde^[35] or 4-(Cy₃PAuC≡C)benzaldehyde^[29] as the starting materials. Combining **7** with azidotrimethylsilane in methanol led to the triazole,^[34] compound **8**. Compound **2** was synthesized by base-promoted auration with **L2**, which was synthesized in a palladium-catalyzed borylation reaction (Scheme 3, step 4).

Compounds **3** and **4** were synthesized as shown in Scheme 4. Sonogashira coupling^[43] of **L1'** or **L3'** with trimethylsilylacetylene afforded a triple bond at the positions of the original Br substituents. These compounds were then de-

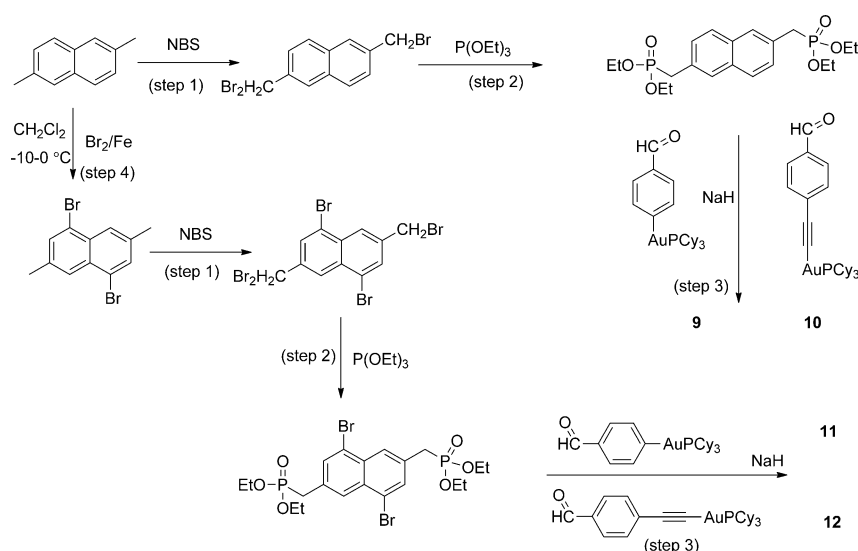
silylated with K₂CO₃ to afford the tetraethynyl distyryl benzene. The products were deprotonated by a strong base, KO^{*t*}Bu, and reacted with Cy₃PAuCl in methanol to yield **3** and **4**.

Attempts to synthesize the triazolato complexes from compound **3** were not successful, possibly due to steric hindrance.^[44]

The corresponding gold(I) distyryl naphthalenes were synthesized in a similar way, shown in Scheme 5. Steps 1–3 are analogous to steps 1–3 in Scheme 3, but with different starting materials. The only step of concern is the iron-catalyzed bromination (Scheme 5, step 4). Here, 2,6-dimethylnaphthalene was first dissolved in CH₂Cl₂ and cooled to –10 °C. Fe powder and a crystal of I₂ were added to the solution, and the mixture was deoxygenated. A solution of Br₂ in methyl-



Scheme 4. Synthesis of **3** and **4**.

Scheme 5. Syntheses of **9–12**.

ene chloride was added, with bubbling of argon. The reaction mixture was kept under Ar, warmed to room temperature, and stirred overnight. Upon completion, the solution was separated from Fe metal using a magnet, and diluted with CH_2Cl_2 . It was then washed with saturated aqueous Na_2SO_3 several times. Rotary evaporation afforded a white solid, which was carefully washed with a small amount of hexanes. Washing with excess hexanes caused the loss of products. Unidentified materials were produced when the reaction mixtures were exposed to air. Further purification can be achieved by crystallizing the product in CHCl_3 .^[45]

Ligand **L1** and compound **1** were isolated as white powders. Compound **1** is soluble in benzene. Diffusing pentane into a saturated benzene solution of compound **1** led to the isolation of colorless crystals. Ligands **L2**, **L3**, **L1'–L3'**, compounds **2**, **3**, **5–7**, and **9–12** were isolated as yellow powders. **L2'** and **L3'** are minimally soluble in dichloromethane or chloroform; **L1'** is more soluble. The digold(I) complexes dissolve in dichloromethane and chloroform. Yellow crystals of **2** were collected by diffusing ether into a saturated CH_2Cl_2 solution. Crystallization of the other compounds only led to the precipitation of yellow powders, which were analytically pure upon drying. The more conjugated compounds **4** and **8** have darker yellow colors. Crystallization led to the formation of orange crystals.

Gold(I) complexes with bromo substituents are less soluble than those without. Direct auration using **L4** to make a tetragold complex with gold(I) fragments σ -bonded to the phenyl ring met with limited success. Product formation could be seen in high-resolution MS, but the compound's sensitivity to ambient light precluded its isolation.

From $^{31}\text{P}\{^1\text{H}\}$ NMR spectroscopy, the formation of $\text{Au}-\text{C}_{\text{aromatic}}$ and $\text{Au}-\text{C}\equiv\text{C}$ bonds could be observed. As shown in Table 1, the $^{31}\text{P}\{^1\text{H}\}$ resonances appear in the expected ranges. Phosphorus resonances of gold(I) alkynyls are shifted slightly upfield relative to those in analogues in which

gold binds directly to benzene rings. The ^{31}P resonance of triazolato complex **8** is shifted downfield. In ^1H NMR spectra, the coupling constants of the doublet of doublets assigned to the alkenyl hydrogens are all about 16.0 Hz, indicating a *trans* geometry according to the Karplus equation. The only exception is **1**. Here, the doublet of doublets of the two alkenyl protons is distinguished from the other peaks.

Figure 1 shows crystal structures for compounds **1** and **4**. The Au^{I} centers adopt a linear, two-coordinate geometry. The bulky tricyclohexylphosphine li-

Table 1. $^{31}\text{P}\{^1\text{H}\}$ chemical shifts of the gold(I) styryl benzene and naphthalene complexes in CDCl_3 .

| Compound | $^{31}\text{P}\{^1\text{H}\}$ [ppm] | Compound | $^{31}\text{P}\{^1\text{H}\}$ [ppm] |
|--------------------------|-------------------------------------|--------------------------|-------------------------------------|
| 1 ^[a] | 57.5 | 3 ^[b] | 56.8 |
| 2 ^[a] | 57.9 | 4 ^[b] | 56.8, 56.7 |
| 5 ^[a] | 57.9 | 7 ^[b] | 56.9 |
| 6 ^[a] | 57.6 | 10 ^[b] | 56.9 |
| 9 ^[a] | 57.8 | 12 ^[b] | 56.9 |
| 11 ^[a] | 57.8 | 8 ^[c] | 58.5 |

[a] Compounds with direct $\text{Au}-\text{C}_{\text{aromatic}}$ bonds. [b] Compounds with $\text{Au}-\text{C}\equiv\text{C}$ bonds. [c] The gold-triazolato compound ($\text{Au}-\text{C}_{\text{triazole}}$).

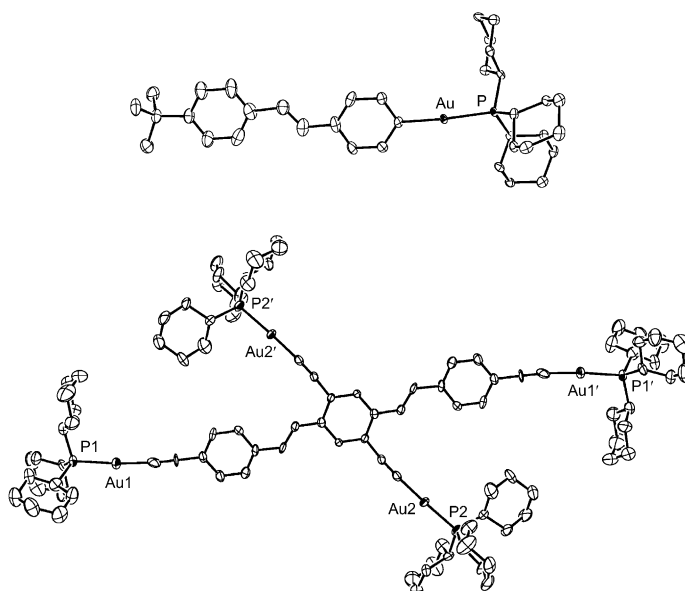


Figure 1. Crystal structures (100 K) of compounds **1** (top) and **4** (bottom); 50% probability ellipsoids are shown. Hydrogen atoms are omitted for clarity. Unlabeled atoms are carbon. One PCy_3 group in the asymmetric unit of **4** is disordered. Co-crystallized solvent molecules are omitted for clarity.

gands preclude aurophilic interactions. One independent molecule resides in the asymmetric unit of the crystal structure of **1**. The asymmetric unit of **4** contains one half-molecule; **4** resides on a crystallographic inversion center. One PCy₃ group in the asymmetric unit of **4** is disordered. Two dichloromethane molecules crystallized in the asymmetric unit of **4**. Both crystal structures show *trans* carbon–carbon double bonds, consistent with the ¹H NMR data. The structure of **4** shows a nonplanar arrangement of the terminal and the central phenyl rings. The dihedral angle between the two best-fit planes along the long and short axis is 14.05°, Figure 2.

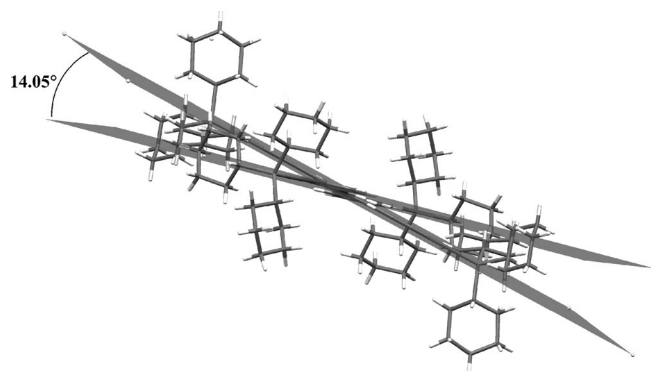


Figure 2. Crystal structure of **4** illustrating the dihedral angle between best fit-planes along the long and short axis.

As seen from Table 2, in compound **1** Au^I forms a σ bond to the aromatic skeleton; the Au–C length is 2.060(6) Å. The two Au–C_{alkynyl} lengths measured in compound **4** are 1.983(13) and 2.001(10) Å, shorter than the Au–C_{aromatic} bonds observed in compound **1**. The \angle C–Au–P angles range from 175.5(3) in one half molecule of compound **4** to 176.02(15) in compound **1**, showing the coordination mode around Au^I is essentially linear.

Table 2. Selected interatomic distances [Å] and angles [°]^[a] in crystallographically characterized gold(I) complexes **1** and **4**.

| | 1 | 4 |
|-------------------------|------------|----------------------|
| Au–C | 2.060(6) | |
| Au–P | 2.3087(15) | 2.261(3), 2.263(3) |
| Au–C _{alkynyl} | | 1.983(13), 2.001(10) |
| C≡C | | 1.172(15), 1.179(13) |
| \angle C–Au–P | 176.03(15) | 175.5(3), 177.6(3) |
| \angle Au–C≡C | | 174.6(10), 176.2(9) |
| \angle C≡C–R | | 175.6(10), 178.7(13) |

[a] The atom in boldface type lies at the vertex of the angle.

Optical spectra: The new gold(I) complexes absorb strongly at wavelengths below 450 nm. They are also luminescent. Figure 3 shows absorption and emission spectra of three representatives: **2**, **5**, and **9**. The normalized absorption spectra of all organogold compounds reported here are collected in Figure S1 in the Supporting Information, and Table 3 sum-

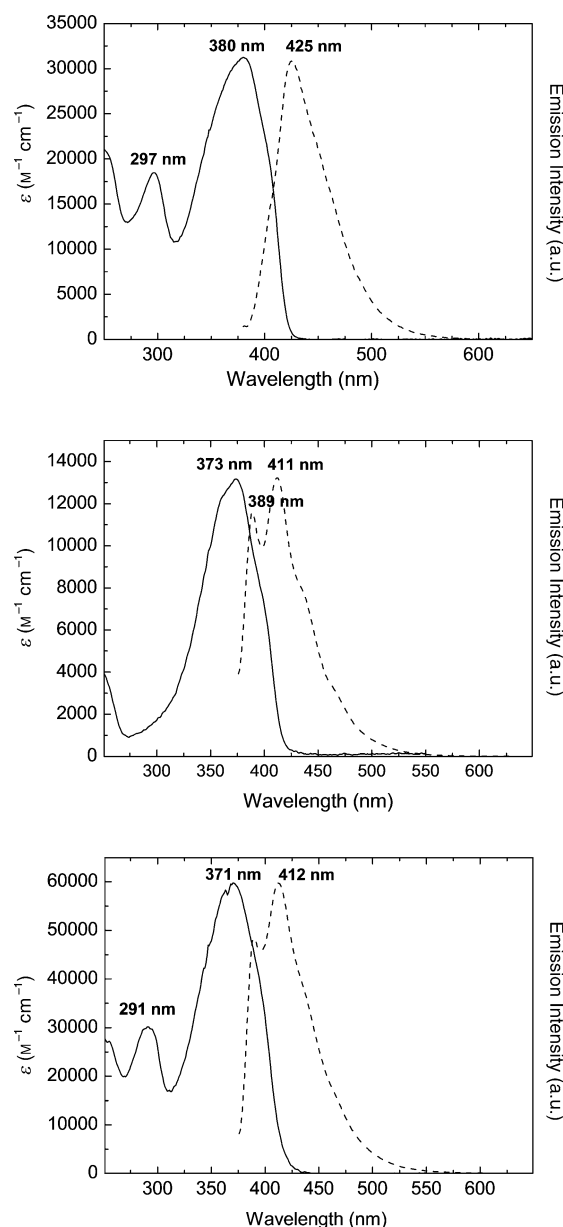


Figure 3. Room-temperature absorption and emission spectra in chloroform of **2** (top), **5** (middle) and **9** (bottom).

marizes absorption maxima and molar absorptivities. Table 4 compiles emission maxima at room temperature. The 0–0 energies ($E_{0,0}$) are readily estimated from the crossing wavelengths of the absorption and emission profiles. For **2**, **5**, and **9**, these are 408, 386, and 388 nm, respectively.

In digold compounds in which the Cy₃PAu^I fragments are σ -bonded to aryl carbons, a strong absorption peak occurs around 380 nm. This peak changes little upon moving the attachment points of Au from the central to the terminal phenyl rings. The digold compound **2** with two gold(I) fragments at the central phenyl ring has another higher energy absorption peak at about 300 nm. The absorption profiles of **5** and **6** are essentially the same, with **6** emitting at longer wavelengths with a more structured emission pattern

Table 3. Absorption maxima and molar absorptivities of new compounds. All spectra were measured in CH_2Cl_2 .

| | λ_{max} [nm] | ϵ [$\text{M}^{-1}\text{cm}^{-1}$] | | λ_{max} [nm] | ϵ [$\text{M}^{-1}\text{cm}^{-1}$] |
|-----------|--------------------------------|---|-----------|--------------------------------|---|
| L1 | 324 | 4.33×10^4 | 6 | 375 | 2.51×10^4 |
| L2 | 369 | 2.58×10^4 | 7 | 279 | 1.92×10^4 |
| L3 | 368 | 5.01×10^4 | 8 | 383 | 4.03×10^4 |
| L4 | 373 | 3.81×10^4 | 1 | 288 | 2.02×10^4 |
| 1 | 330 | 3.95×10^4 | | 378 | 3.07×10^4 |
| 2 | 297 | 1.85×10^4 | 9 | 291 | 3.04×10^4 |
| | 380 | 3.13×10^4 | 10 | 371 | 6.00×10^4 |
| 3 | 324 | 4.53×10^4 | 11 | 279 | 1.92×10^4 |
| | 371 | 2.35×10^4 | 12 | 383 | 4.03×10^4 |
| 4 | 282 | 3.37×10^4 | 11 | 245 | 7.40×10^3 |
| | 333 | 6.94×10^4 | | 300 | 6.12×10^3 |
| | 389 | 4.85×10^4 | | 315 | 3.18×10^4 |
| 5 | 373 | 1.32×10^4 | | 389 | 4.53×10^4 |

Table 4. Emission maxima and quantum yields (ex. 325 nm, standard: anthracene, $\phi=0.27$ in ethanol) of gold(I) styrylbenzene and -naphthalene complexes. Compounds **5** and **9** are highly emissive, and their quantum yields were calculated using 7-diethylamino-4-methylcoumarin (ex. 325 nm, $\phi=0.56$ in ethanol) as the standard. Estimated error in quantum yields: $\pm 10\%$.

| Compound | λ_{ex} [nm] | E_{m} [nm] | ϕ |
|-----------|----------------------------|---------------------|--------|
| 1 | 325 | 357, 374 | 0.054 |
| 2 | 371 | 427 | 0.026 |
| 3 | 371 | 427 | 0.024 |
| 4 | 389 | 447, 468 | 0.124 |
| 5 | 373 | 389, 411 | 0.574 |
| 6 | 375 | 403, 429, 455 | 0.071 |
| 7 | 383 | 421, 448 | 0.063 |
| 8 | 378 | 462 | 0.010 |
| 9 | 371 | 400, 412 | 0.944 |
| 10 | 383 | 417, 435 | 0.034 |
| 11 | 380 | 430, 454 | 0.023 |
| 12 | 389 | 415, 440 | 0.151 |

(Table 3). Compounds **3** and **4** have similar absorption patterns, with one higher energy absorption at about 330 nm, and a lower energy peak at 400 nm. Both the absorption and emission of compound **4** experience obvious red shifts compared with compound **3**. This red shift occurs with the expansion of the conjugation system incorporating $\text{C}\equiv\text{C}$ bonds (**3**, **4**, **7**, **10**, and **12**). In contrast to **6**, compound **7** has another low intensity absorption peak at about 275 nm. The absorption at longer wavelength experiences an approximate 10 nm red shift. Their emission patterns are similar. The triazolate compound **8** has a similar absorption profile to compound **7**, with the shorter wavelength absorption blue-shifting to 255 nm. It emits at a comparatively long wavelength, similar to the tetragold alkynyl compound **4**. There is no dramatic change in either the absorption or emission profiles when substituting the central phenyl ring with a naphthalene ring.

As seen from Figure 4, the color of the compounds varies with structure. The monogold compound **1** is colorless in solution. Compounds **5**, **2**, **4**, and **8** are arranged in an order of intensifying colors. Compounds **4** and **8** are dark orange in

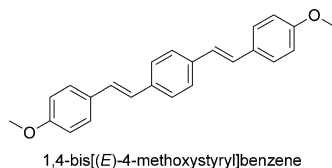


Figure 4. Top: Photograph of compounds **1**, **5**, **2**, **4** and **8** arranged by the intensity of their colors in dichloromethane. Bottom: Emission under 254 nm irradiation.

the solid state. These compounds are blue-light emitters. The blue emission of the tetragold alkynyl compound **4** interferes with the solution color, and a green emission is seen, Figure 4. These colors can be clearly seen under UV light in the dark. Their emission quantum yields (included in Table 3) show structural correlations. The new compounds tend to have higher emission quantum yields when the gold fragments bind the ends of the conjugated system, as seen from the high quantum yields of compounds **5** and **9** in Table 3 and the bright blue emission of **5** in Figure 4. The blue emissions of compound **2** and **8** are inconspicuous, consistent with their relatively lower quantum yields. At high concentrations, the blue emission of **8** is concealed by the dark orange color of the solution. At lower concentrations, a green color can be observed as seen in compound **4**. When dissolving these compounds in a mixture of dichloromethane and methanol, the emission colors experience no change, showing negligible solvent effects on the luminescence.

Substituting terminal hydrogen atoms with gold(I) fragments red-shifts the absorption profile of the parent hydrocarbon. We have made similar observations for related mono- and digold(I) aryls.^[46] Cornil and co-workers^[47] have reported that *para*-distyrylbenzene, the hydrocarbon parent of **5**, shows an absorption maximum at 365 nm in a poly-(methyl methacrylate) film. Wu and co-workers^[48] report the absorption spectrum of the same hydrocarbon in chloroform; it has a maximum at 368 nm (estimated from the printed spectrum). Substitution of **5** with alkyl, alkoxy, and dialkylamino groups red-shifts the absorption profile. How-

ever, the degree of red-shifting is not simply related to the electron-donating power of the substituent. The absorption maximum of 1,4-bis[(*E*)-4-methoxystyryl]benzene near



369 nm in CHCl₃ is similar to that of **5** (373 nm, in CH₂Cl₂). This observation need not suggest that (phosphine)gold(I) substituents are electron-releasing. Boronated compound **L3** absorbs at 385 nm in CH₂Cl₂. Time-dependent density-functional theory calculations^[46] have suggested that this red-shift results from configuration interaction involving gold-based orbitals that moves singlet excited states to lower energies.

Spectral comparisons can be made among the new compounds. For example, **6** is the dibromo analogue of **5**, in which the central benzene ring is brominated. However, the absorption maxima in CH₂Cl₂ change little: 373 (**5**) vs. 375 nm (**6**). Similarly, bromine substitution on the naphthalene cores of **11** and **12** has little effect on their absorption profiles. In compounds **6**, **7**, and **8**, gold binds directly to an aromatic ring (**6**), through an alkynyl spacer (**7**), and through a triazolato ring (**8**). For further comparison, **L3** is the pinacolboronate precursor to **6**. The lowest-energy absorption maxima of these compounds in CH₂Cl₂ span a 15 nm range and increase in order: **L3** (368) < **6** (325) < **8** (378) < **7** (383 nm). Gold(I) leads to greater red-shifting than boronate esters, but absorption wavelengths are not a simple function of conjugation length. Still, variations within the series are not large.

The fluorescence quenching effect of the heavy atom (Br) rationalizes the lower quantum yield of **11** compared to **9**. The quenching effect of gold appears to be more effective in the alkynyl **7** than in a triazolato system **8**. Comparing **9** and **10**, or **11** and **12**, shows a drastic decrease in fluorescence quantum yield when adding an alkynyl spacer between gold and the two terminal aryl carbons of the conjugated bridge. However, the fluorescence quantum yields are insensitive to similar changes on the central aromatic ring, as seen from comparing **2** and **3**, as well as **6** and **7**. Compound **4** has a higher emission quantum yield than **7**, indicating stronger quenching by Br than by the gold alkynyl fragment.

Calculations: Compounds **2**, **5**, and **9** were selected for theoretical investigation. For computational feasibility, PMe₃ ligands replace PCy₃ on gold. Model compounds are denoted with primes: **2'**, **5'**, and **9'**.

Geometries were optimized free of imposed symmetry. Harmonic frequency calculations show the converged structures to be minima of the potential energy hypersurface. All calculations, including geometry optimizations, incorporate

chloroform solvation, modeled with the IEFPCM formalism of Tomasi and co-workers.^[49–52]

Figure 5 (top) shows a frontier-orbital energy level diagram of **5'**. Images of the highest occupied and lowest unoccupied Kohn–Sham orbitals (HOMO and LUMO, respec-

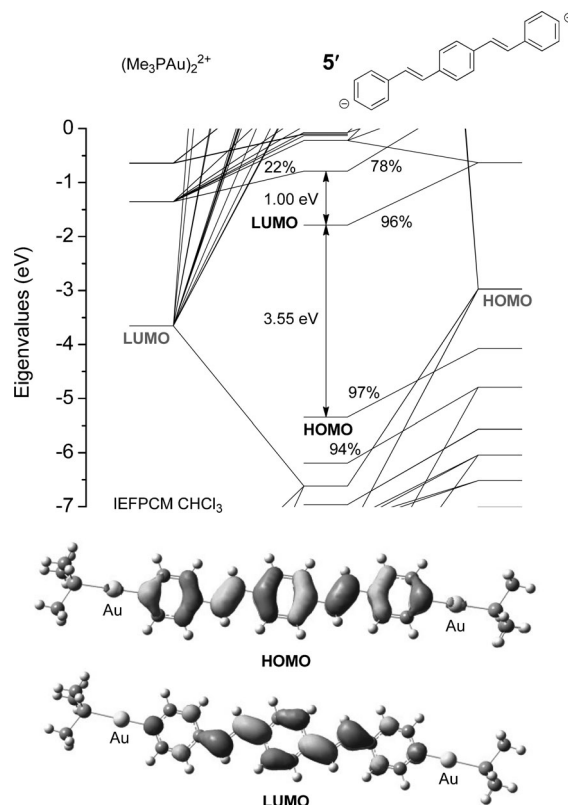


Figure 5. Top: Partial Kohn–Sham orbital energy level diagram of model **5'** in continuum (IEFPCM) chloroform solvation. Percentage compositions of selected orbitals, in terms of fragment orbitals, are indicated. Bottom: Plots of the highest occupied and lowest unoccupied orbitals of **5'**. The contour level is 0.03 a.u.

tively) appear in Figure 5 (bottom). The corresponding diagrams for **9'** are given in Figure 6; a diagram for **2'** appears in Figure S2 in the Supporting Information. Percentage compositions in terms of fragment orbitals are indicated; these derive from a Mulliken population analysis.^[53]

In **5'**, the highest occupied orbital with significant gold character is the HOMO–2, which, along with the HOMO–3, accounts for the carbon–gold σ bonds. For **9'**, the HOMO–3 and the HOMO–4 are the highest-lying filled orbitals with large gold character. Other orbitals near the frontier are mainly π orbitals of the conjugated bridge. Similar conclusions pertain to the electronic structure of **2'**.

Time-dependent DFT calculations for **2'**, **5'**, and **9'** find that the first excited singlet states result from clean LUMO \leftarrow HOMO promotions. This transition is optically allowed for both molecules. The corresponding absorption is intense, and the calculations predict it to have the highest oscillator strength of any transition up to 300 nm. We note

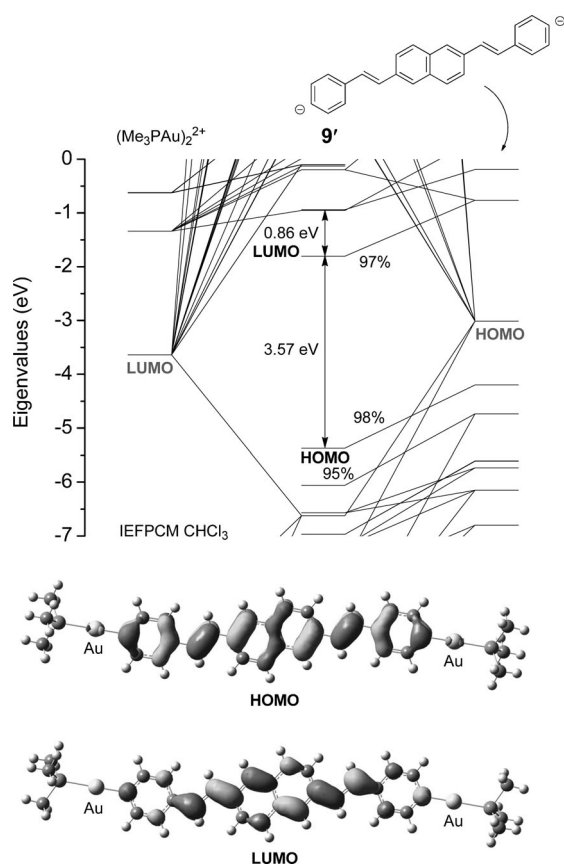


Figure 6. Top: Partial Kohn–Sham orbital energy level diagram of model **9'** in continuum (IEFPCM) chloroform solvation. Percentage compositions of selected orbitals, in terms of fragment orbitals, are indicated. Bottom: Plots of the highest occupied and lowest unoccupied orbitals of **9'**. The contour level is 0.03 a.u.

that the emission spectra of **5** and **9** show the structured luminescence typical of aryl-ligand-centered emission.^[30–32,35] Table 5 collects the calculated vertical excitation energies and compositions of singlet excited states up to 300 nm for **2'**, **5'**, and **9'**. Excitation energies calculated for the first singlet excited states agree well with observed 0–0 energies (within 8%). Higher-energy singlets, and all triplets within this energy range, mix through configuration interaction, and are not described by simple one-electron transitions.

Conclusion

Gold(I) styrylbenzene, distyrylbenzene and distyrylnaphthalene complexes were synthesized and characterized. In the synthesis of these compounds, base-promoted auration, alkylation and [3+2] cycloaddition methods, as well as Horner–Wadsworth–Emmons reactions, were used. Different distyryl benzene and naphthalene bridges were designed. Gold(I) is attached to different places along the conjugated backbones, either directly or with alkyne or triazolone spacers. In some systems, bromo substituents are also present. All these compounds are air and water stable.

Table 5. Compositions and energies of singlet excited states calculated by TDDFT, with estimated 0–0 energies, $E_{0,0}$, for comparison.

| No. | E [nm] | F | Orbital origin (percentage contribution) |
|-----------------------------------|-------------|--------|---|
| compound 2' singlet states | | | |
| 1 | 412.9 | 1.5954 | HOMO→LUMO (+98%) |
| 2 | 347.6 | 0.0100 | HOMO–1→LUMO (+96%) |
| 3 | 322.1 | 0.0515 | HOMO–3→LUMO (+72%) HOMO→LUMO+2 (22%) |
| 4 | 318.1 | 0.0002 | HOMO→LUMO+1 (+96%) |
| 5 | 307.6 | 0.0003 | HOMO–2→LUMO (+93%) |
| 6 | 301.1 | 0.8817 | HOMO→LUMO+2 (+75%) HOMO–3→LUMO (+21%) |
| compound 5' singlet states | | | |
| 1 | 418.4 | 2.6363 | HOMO→LUMO (+98%) |
| 2 | 321.5 | 0.0001 | HOMO–1→LUMO (+90%) HOMO→LUMO+1 (8%) |
| 3 | 306.5 | 0.0003 | HOMO→LUMO+1 (+89%) HOMO–1→LUMO (+8%) |
| compound 9' singlet states | | | |
| 1 | 412.8 | 3.0594 | HOMO→LUMO (+97%) |
| 2 | 343.2 | 0.0056 | HOMO→LUMO+2 (+76%) HOMO–2→LUMO (21%) |
| 3 | 330.1 | 0 | HOMO–1→LUMO (+96%) |
| 4 | 316.1 | 0 | HOMO→LUMO+1 (+95%) |

The syntheses of these compounds were verified by NMR, HR-MS and X-ray crystallography. The ³¹P{¹H} NMR data indicate the formation of gold–carbon bonds. When the gold fragments are directly σ -bonded to the aromatic carbons, ³¹P{¹H} chemical shifts are near 58 ppm. When an alkyne spacer intervenes between gold and an aromatic ring, the ³¹P{¹H} peaks appear near 56 ppm. In ¹H NMR spectra, the coupling constants of about 16.0 Hz for the doublet of doublets assigned to the protons of the ethylene spacers show that all these compounds are *trans* isomers. Crystal structures show a linear geometry of the gold(I) centers. No short Au–Au interactions were observed.

As the conjugation length increases, the color of the solid compounds intensifies. The monogold(I) compound is colorless, and the digold(I) complexes change from yellow to orange. The tetragold(I) compound is dark orange. With more bromo substituents, the solubility of the compounds decreases. All these complexes absorb UV light strongly, and emit from 350–460 nm. These emissions are not quenchable by oxygen, and no triplet state emission was observed at room temperature. Fluorescence quantum yields vary with structure. The highest quantum yields occur when attaching two gold fragments directly to the two ends of the conjugated system. When there is an alkyne spacer between gold and the conjugated bridge, the quantum yield decreases. The heavy atom effects of gold(I) and bromo substituents quench fluorescence, as expected for intersystem crossing to triplet excited states. Quenching is less efficient in the triazolone system than in the alkyne system. Time-dependent density-functional theory calculations indicate that the emission of these compounds derives from the conjugated aromatic moiety.

The emissive compounds herein can be used as blue emitters, and potentially as two-photon absorbers.

Experimental Section

Reagents: Commercially available reagents were used as received without further purification. [(Cy₃P)Au(4-formylphenyl)] was synthesized based on a base-promoted auration procedure as reported.^[30] Cy₃PAuBr and [(Cy₃P)Au(4-ethynylphenyl)] were synthesized following literature procedures.^[29,54]

NMR spectroscopy: NMR spectra (¹H, ¹³C{¹H}, and ³¹P{¹H}) were recorded on a Varian AS-400 spectrometer. Chemical shifts are reported in ppm relative to Si(CH₃)₄ (¹H, ¹³C{¹H}) or 85% aqueous H₃PO₄ (³¹P{¹H}).

Elemental analysis and mass spectrometry: Microanalyses (C, H, and N) were performed by Robertson Microlit Laboratories. Mass spectrometry was performed at the University of Cincinnati Mass Spectrometry facility. We have not obtained satisfactory elemental analyses for compounds **6**, **10**, and **11**; these substances have been characterized by high-resolution mass spectrometry.

Optical properties characterization: UV/Vis spectra were collected on a Cary 500 spectrophotometer in degassed HPLC-grade solvents. Fluorescence measurements were done with a Cary Eclipse Spectrophotometer at room temperature. All the luminescence spectra were collected both in the air and after being purged with argon.

X-ray structure determinations: Single-crystal X-ray data were collected on a Bruker AXS SMART APEX CCD diffractometer using monochromatic MoK_α radiation with the omega scan technique. The unit cells were determined using SMART^[55] and SAINT+. Data collection for all crystals was conducted at 100 K (−173.5°C). All structures were solved by direct methods and refined by full matrix least squares refinement against F² with all reflections using SHELXTL. Refinement of extinction coefficients was found to be insignificant. All non-hydrogen atoms were refined anisotropically. All hydrogen atoms were placed in standard calculated positions and all hydrogen atoms were refined with an isotropic displacement parameter 1.2 times that of the adjacent carbon. CCDC-871911 (**4**) and CCDC-871912 (**1**), contain the supplementary crystallographic data for this paper. These data can be obtained free of charge from The Cambridge Crystallographic Data Centre via www.ccdc.cam.ac.uk/data_request/cif.

Synthesis of ligands and gold(I) complexes

1,4-Dibromo-2,5-bis(4-*tert*-butylstyryl)benzene (L1'): Tetraethyl[(2,5-dibromo-1,4-phenylene)bis(methylene)]bis(phosphonate) (3.0 g, 5.6 mmol) and 4-*tert*-butylbenzaldehyde (2.0 g, 12.3 mmol) were combined in THF (30 mL). NaH (0.54 g, 13.4 mmol) was added, and the resulting suspension was refluxed for 3 h. After cooling to RT, ice was added to the reaction mixture and stirred vigorously to generate a fine yellow suspension. Vacuum filtration led to the isolation of a yellow powder, which was washed several times with THF and water, and dried under vacuum. Yield: 1.90 g, 61%; ¹H NMR (CDCl₃): δ = 7.87 (s, 2H), 7.50 (d, *J* = 8.4 Hz, 4H), 7.42 (d, *J* = 8.4 Hz, 4H), 7.33 (d, *J* = 16.0 Hz, 2H), 7.04 (d, *J* = 16.4 Hz, 2H), 1.34 ppm (s, 18H).

1,4-Dibromo-2,5-bis(4-bromostyryl)benzene (L3'): Tetraethyl[(2,5-dibromo-1,4-phenylene)bis(methylene)]bis(phosphonate) (3.0 g, 5.6 mmol) and 4-bromo-benzaldehyde (2.3 g, 12.3 mmol) were combined in THF (30 mL); NaH (0.54 g, 13.4 mmol) was added. The resulting suspension was refluxed for 3 h. After cooling to RT, ice was added to the reaction mixture and stirred vigorously to generate a fine yellow suspension. Vacuum filtration led to the isolation of a yellow powder, which was washed several times with THF and water, and dried under vacuum. This material is minimally soluble in chloroform. Yield: 1.0 g, 57%; ¹H NMR (CDCl₃): δ = 7.68 (s, 2H), 7.28 (d, *J* = 15.6 Hz, 4H), 7.23 (d, *J* = 8.4 Hz, 4H), 6.89 (d, *J* = 8.4 Hz, 2H), 6.42 ppm (d, *J* = 16.0 Hz, 2H).

These materials were pure by an NMR criterion and were used without further purification.

(E)-2-[4-(4-*tert*-Butylstyryl)phenyl]-4,4,5,5-tetramethyl-1,3,2-dioxaborolane (L1): [Pd(dba)₂] (3 mol%, 0.0096 g, 0.017 mmol) and PCy₃ (7.2 mol%, 0.0112 g, 0.040 mmol) were combined in degassed 1,4-dioxane (5 mL), and stirred for 30 min. 1-Bromo-4-(4-*tert*-butylstyryl)benzene (0.1750 g, 0.555 mmol), bis(pinacolato)diboron (B₂pin₂, 0.1551 g, 0.610 mmol) and KOAc (0.0081 g, 0.834 mmol) were added to this solu-

tion. The resulting mixture was transferred out of the box and heated under Ar in an 80°C oil bath overnight. Solvent was removed under rotary evaporation. Vacuum sublimation led to the isolation of white crystals as the pure product. Yield: 0.1277 g, 63%; ¹H NMR (CDCl₃): δ = 7.79 (d, *J* = 8.0 Hz, 2H), 7.51 (d, *J* = 8.0 Hz, 2H), 7.47 (d, *J* = 8.4 Hz, 2H), 7.39 (d, *J* = 8.4 Hz, 2H), 7.17 (d, *J* = 16.4 Hz, 1H), 7.08 (d, *J* = 16.4 Hz, 1H), 1.34 ppm (d, *J* = 8 Hz, 21H); m.p. 183–184°C; elemental analysis calcd (%) for C₂₃H₃₀BO₂: C 79.09, H 8.66; found: C 79.33, H 8.39; UV/Vis (CH₂Cl₂): λ (ε) = 324 nm (4.33 × 10⁴ m^{−1} cm^{−1}); emission (CH₂Cl₂, ex. 324 nm): λ = 373 nm.

2,2'-(2,5-Bis[(E)-4-(4-*tert*-butylstyryl)-1,4-phenylene]bis(4,4,5,5-tetramethyl-1,3,2-dioxaborolane) (L2): [Pd(dba)₂] (6 mol%, 0.0173 g, 0.030 mmol) and PCy₃ (14 mol%, 0.0202 g, 0.072 mmol) were combined in 1,4-dioxane (5 mL) in a nitrogen glove box, and stirred for 30 min. 1,4-Dibromo-2,5-bis(4-*tert*-butylstyryl)benzene (0.2706 g, 0.490 mmol), bis(pinacolato)diboron (B₂pin₂, 0.1912 g, 0.753 mmol) and KOAc (0.1428 g, 1.47 mmol) were added to this solution. The resulting mixture was heated under Ar in an 80°C oil bath overnight. Solvent was removed under rotary evaporation. The resulting residue was dissolved in CH₂Cl₂ and washed with water twice. The CH₂Cl₂ layer was collected and dried over MgSO₄. Solvent was then removed under rotary evaporation, leaving a yellow powder. The powder was then dissolved in a minimum amount of CH₂Cl₂, and methanol was added until turbidity was seen. The suspension was allowed to stand for further precipitation. Vacuum filtration led to the isolation of the product as a yellow powder. Yield: 0.1678 g, 53%; ¹H NMR (CDCl₃): δ = 8.16 (s, 2H), 7.99 (d, *J* = 16.4 Hz, 2H), 7.50 (d, *J* = 8.0 Hz, 2H), 7.39 (d, *J* = 8.0 Hz, 2H), 7.12 (d, *J* = 16.4 Hz, 2H), 1.43 (s, 24H), 1.35 ppm (s, 18H); m.p. 294°C (decomp); UV/Vis (CH₂Cl₂): λ (ε) = 369 nm (2.58 × 10⁴ m^{−1} cm^{−1}); emission (CH₂Cl₂, ex. 369 nm): λ = 410, 430 nm.

1,4-Bis[(E)-4-(4,4,5,5-tetramethyl-1,3,2-dioxaborolan-2-yl)styryl]benzene (L3): [Pd(dba)₂] (6 mol%, 0.0120 g, 0.021 mmol) and PCy₃ (14 mol%, 0.0143 g, 0.051 mmol) were combined in 1,4-dioxane (5 mL) in a nitrogen glove box, and stirred for 30 min. 1,4-Bis(4-bromostyryl)benzene (0.1536 g, 0.350 mmol), bis(pinacolato)diboron (B₂pin₂, 0.1950 g, 0.768 mmol) and KOAc (0.1017 g, 1.05 mmol) were added to this solution. The resulting mixture was transferred out of the box and heated under Ar in an 80°C oil bath overnight. Solvent was removed under rotary evaporation. The resulting residue was dissolved in CH₂Cl₂ and washed with water twice. The CH₂Cl₂ layer was collected and dried over MgSO₄. Solvent was then removed under rotary evaporation, leaving a yellow powder. The powder was then dissolved in a minimum amount of CH₂Cl₂, and methanol was added until turbidity was seen. The suspension was allowed to stand for further precipitation. Vacuum filtration led to the isolation of the product as a yellow powder. Yield: 0.1237 g, 53%; ¹H NMR (CDCl₃): δ = 7.80 (d, 4H, *J* = 8 Hz), 7.51–7.54 (m, 8H), 7.19 (d, 2H, *J* = 16.0 Hz), 7.13 (d, 2H, *J* = 16.0 Hz), 1.36 ppm (s, 24H); m.p. 306°C (decomp); UV/Vis (CH₂Cl₂): λ (ε) = 368 nm (5.01 × 10⁴ m^{−1} cm^{−1}); emission (CH₂Cl₂, ex. 369 nm): λ = 403, 427 nm.

2,2'-(2,5-Bis[(E)-4-(4,4,5,5-tetramethyl-1,3,2-dioxaborolan-2-yl)styryl]-1,4-phenylene)bis(4,4,5,5-tetramethyl-1,3,2-dioxaborolane) (L4): [Pd(dba)₂] (12 mol%, 0.0143 g, 0.0249 mmol) and PCy₃ (28 mol%, 0.0167 g, 0.060 mmol) were combined in 1,4-dioxane (5 mL) in the glove box, and stirred for 30 min. 1,4-Dibromo-2,5-bis(4-bromostyryl)benzene (0.1240 g, 0.207 mmol), bis(pinacolato)diboron (B₂pin₂, 0.2317 g, 0.912 mmol) and KOAc (0.1209 g, 1.24 mmol) were added to this solution. The resulting mixture was heated under Ar in an 80°C oil bath overnight. Solvent was removed under rotary evaporation. The resulting residue was dissolved in CH₂Cl₂ and washed with water twice. The CH₂Cl₂ layer was collected and dried over MgSO₄. Solvent was then removed under rotary evaporation, leaving an orange powder. The powder was then dissolved in a minimum amount of CH₂Cl₂, and methanol was added until turbidity was seen. The suspension was allowed to stand for further precipitation. Vacuum filtration led to the isolation of the product as an orange crystalline material. Yield: 0.060 g, 36%; ¹H NMR (CDCl₃): δ = 8.17 (s, 2H), 8.11 (d, *J* = 16.0 Hz, 2H), 7.81 (d, *J* = 8.0 Hz, 4H), 7.56 (d, *J* = 8.0 Hz, 4H), 7.15 (d, *J* = 16.4 Hz, 2H), 1.41 (s, 24H), 1.36 ppm (s, 24H); m.p.

294–296 °C (decomp); UV/Vis (CH₂Cl₂): λ (ϵ) = 373 nm ($3.81 \times 10^4 \text{ M}^{-1} \text{ cm}^{-1}$); emission (CH₂Cl₂, ex. 373 nm): λ = 414, 437, 463 nm.

These materials were pure by an NMR criterion and used without further purification.

(E)-1-[(Cy₃P)Au]-4-(4-*tert*-butylstyryl)benzene (1): [(Cy₃P)AuBr] (0.0923 g, 0.166 mmol), **L1** (0.0900 g, 0.25 mmol), Cs₂CO₃ (0.1619 g, 0.50 mmol) were suspended in isopropyl alcohol (10 mL) and charged into a round bottom flask. After degassing, the reaction vessel was immersed in a 50 °C oil bath, and stirred under Ar for 24 h. After cooling, isopropyl alcohol was removed under rotary evaporation, and the remaining solid was extracted into benzene (50 mL) and filtered through Celite. The solution was put under a rotary evaporator and benzene was removed. The residue was triturated with pentane. Vacuum filtration gave the product as a white powder. The white powder was then dissolved in a minimum amount of benzene and filtered through Celite. Diffusing pentane into the concentrated benzene solution afforded the product as colorless crystals. Yield: 0.1000 g, 85%; ¹H NMR (C₆D₆): δ = 8.13–8.17 (m, 2H), 7.69 (d, J = 7.6 Hz, 2H), 7.40 (d, J = 8 Hz, 2H), 7.20–7.27 (m, 4H); 1.34–1.85 (m, 24H, (C₆H₁₁)₃), 1.24 (s, 9H, *tert*-butyl), 1.00–1.05 ppm (m, 9H, (C₆H₁₁)₃); ³¹P{¹H} NMR (C₆D₆): δ = 57.5 ppm; HR-MS (ES⁺): m/z calcd: 713.3550 [$M+H$]⁺; found: 713.3632; elemental analysis calcd (%) for C₂₆H₃₂AuP: C 60.67, H 7.35; found: C 60.41, H 7.31; UV/Vis (2-MeTHF): λ (ϵ) = 288 (3.65×10^4), 330 nm ($3.95 \times 10^4 \text{ M}^{-1} \text{ cm}^{-1}$); emission (2-MeTHF, ex. 325 nm): λ = 357, 374 nm.

1,4-Bis[(Cy₃P)Au]-2,5-bis(4-*tert*-butylstyryl)benzene (2): [(Cy₃P)AuBr] (0.0794 g, 0.142 mmol), **L2** (0.0506 g, 0.076 mmol), Cs₂CO₃ (0.1022 g, 0.31 mmol) were suspended in isopropyl alcohol (10 mL) and charged into a round bottom flask. Benzene (5 mL) was then added to promote dissolution of the starting materials. After degassing, the reaction vessel was immersed in a 45 °C oil bath, and stirred under Ar for 24 h. After cooling, the solvents were removed under rotary evaporation, and the remaining solid was extracted into dichloromethane (100 mL) and filtered through Celite. The solution was evaporated to dryness. The residue was triturated with pentane. Vacuum filtration gave the product as a yellow powder. The yellow powder was then dissolved in a minimum amount of dichloromethane and filtered through Celite. Diffusing ether into the concentrated dichloromethane solution afforded the product as yellow crystals. Yield: 0.0640 g, 67%; ¹H NMR (CDCl₃): δ = 7.89–7.91 (m, 2H), 7.78 (d, J = 16.0 Hz, 2H), 7.44 (d, J = 8.4 Hz, 4H), 7.29 (d, J = 8.4 Hz, 4H), 7.14 (d, J = 16.0 Hz, 2H), 1.55–2.08 (m, 66H; 2(C₆H₁₁)₃), 1.32 ppm (s, 18H, *tert*-butyl); ³¹P{¹H} NMR (CDCl₃): δ = 57.9 ppm; HR-MS (ES⁺): m/z calcd: 1348.6587 [$M+H$]⁺; found: 1348.6978; elemental analysis calcd (%) for C₆₆H₉₈Au₂P₂: C 58.83, H 7.33; found: C 58.72, H 7.19; UV/Vis (CH₂Cl₂): λ (ϵ) = 297 (1.85×10^4), 380 nm ($3.13 \times 10^4 \text{ M}^{-1} \text{ cm}^{-1}$); emission (CH₂Cl₂ ex. 380 nm): λ = 425 nm.

2,5-Bis(4-*tert*-butylstyryl)-1,4-bis[(Cy₃P)Au]ethynylbenzene (3): [(Cy₃P)AuCl] (85.2 mg, 0.166 mmol) was suspended in methanol (5 mL). KORBu (17.1 mg, 0.153 mmol) and 1,4-diethynyl-2,5-bis(4-*tert*-butylstyryl)benzene (36.4 mg, 0.082 mmol) were combined in methanol (5 mL), and the mixture was then added to the suspension of Cy₃PAuCl. The resulting suspension was stirred at room temperature overnight. The solvent was removed by rotary evaporation. The residue was extracted with CH₂Cl₂ and filtered through a layer of Celite. CH₂Cl₂ was then removed by rotary evaporation, and the resulting solid was triturated with pentane. Diffusing pentane into a saturated CHCl₃ solution yielded a yellow powder, which was washed with pentane and dried under vacuum. Yield: 0.0681 g, 60%; ¹H NMR (CDCl₃): δ = 7.83 (s, 2H), 7.78 (d, J = 16.4 Hz, 2H), 7.51 (d, J = 8.4 Hz, 4H), 7.34 (d, J = 8.8 Hz, 4H), 7.14 (d, J = 16.4 Hz, 2H), 1.43–2.05 ppm (m, 66H); ³¹P{¹H} NMR (400 MHz, CDCl₃) δ = 56.8 ppm (s); MS (ES⁺): m/z calcd: 1395.6475 [$M+Na$]⁺; found: 1395.7225; elemental analysis calcd (%) for C₇₀H₉₈Au₂P₂: C 60.25, H 7.08; found: C 59.97, H 6.80; UV/Vis (CH₂Cl₂): λ (ϵ) = 324 (4.53×10^4), 371 nm ($2.35 \times 10^4 \text{ M}^{-1} \text{ cm}^{-1}$); emission (CH₂Cl₂ ex. 371 nm): λ = 427 nm.

2,5-Bis(4-[(Cy₃P)Au]ethynylstyryl)-1,4-bis[(Cy₃P)Au]ethynylbenzene (4): [(Cy₃P)AuCl] (113.4 mg, 0.221 mmol) was suspended in methanol (5 mL). 1,4-Diethynyl-2,5-bis(4-ethynylstyryl)benzene (20.4 mg, 0.054 mmol) and KORBu (24.2 mg, 0.216 mmol) were also combined in MeOH (5 mL), and the mixture was then added to the suspension of

Cy₃PAuCl. The resulting suspension was stirred at room temperature overnight. The solvent was removed by rotary evaporation. The residue was extracted with CH₂Cl₂ and filtered through a layer of Celite. The solvent was then removed by rotary evaporation, and the resulting solid was triturated with pentane. Diffusion of pentane into a saturated CHCl₃ solution yielded orange crystals. The crystals were washed with pentane and dried under vacuum as the pure product. Yield: 0.1193 g, 96%; ¹H NMR (CDCl₃): δ = 7.81 (s, 2H), 7.76 (d, J = 16.4 Hz, 2H), 7.41–7.45 (m, 4H), 7.11 (d, J = 16.0 Hz, 2H), 7.14 (d, J = 16.4 Hz, 2H), 1.50–2.02 ppm (m, 132H); ³¹P{¹H} NMR (400 MHz, CDCl₃): δ = 56.852 (s), 56.742 ppm (s); MS (MALDI): m/z calcd: 2284.03 [M]⁺; found: 2284.7; elemental analysis calcd (%) for C₁₀₂H₁₄₆Au₄P₄: C 53.64, H 6.44; found: C 53.38, H 6.19; UV/Vis (CH₂Cl₂): λ (ϵ) = 282 (3.37×10^4), 333 (6.94×10^4), 389 nm ($4.85 \times 10^4 \text{ M}^{-1} \text{ cm}^{-1}$); emission (CH₂Cl₂ ex. 389 nm): λ = 447, 468 nm.

1,4-Bis(4-[(Cy₃P)Au]styryl)benzene (5): [(Cy₃P)AuBr] (0.0743 g, 0.133 mmol), **L3** (0.0392 g, 0.071 mmol), and Cs₂CO₃ (0.0956 g, 0.29 mmol) were suspended in isopropyl alcohol (10 mL) and charged into a round bottom flask. Benzene (5 mL) was then added to promote dissolution of the starting materials. After degassing, the reaction vessel was immersed in a 45 °C oil bath, and stirred under Ar for 24 h. After cooling, the solvents were removed under rotary evaporation, and the remaining solid was extracted into dichloromethane (100 mL) and filtered through Celite. Solvent was removed by rotary evaporation. The residue was triturated with pentane. Vacuum filtration gave the product as a yellow powder. The yellow powder was then dissolved in a minimum amount of dichloromethane and filtered through Celite. Diffusing ether into the concentrated dichloromethane solution afforded the product as yellow crystals. Yield: 0.050 g, 61%; ¹H NMR (CDCl₃): δ = 7.49–7.53 (m, 4H), 7.46 (s, 3H), 7.42 (d, J = 6.8 Hz, 4H), 7.37 (d, J = 0.8 Hz, 1H), 7.06 (dd, J = 24.4, 16.8 Hz, 2H), 1.52–2.06 ppm (m, 66H; 2(C₆H₁₁)₃); ³¹P{¹H} NMR (CDCl₃): δ = 57.9 ppm; HR-MS (ES⁺): m/z calcd: 1235.5439 [$M+H$]⁺; found: 1235.5647; elemental analysis calcd (%) for C₅₈H₈₂Au₂P₂: C 56.40, H 6.69; found: C 56.66, H 6.59; UV/Vis (CH₂Cl₂): λ (ϵ) = 373 nm ($1.32 \times 10^4 \text{ M}^{-1} \text{ cm}^{-1}$); emission (CH₂Cl₂ ex. 373 nm): λ = 389, 411 nm.

2,5-Bis(4-[(Cy₃P)Au]styryl)-1,4-dibromobenzene (6): 4-[(Cy₃P)Au]benzaldehyde (0.0890 g, 0.133 mmol) and tetraethyl[(2,5-dibromo-1,4-phenylene)bis(methylene)]bis(phosphonate) (0.0410 g, 0.076 mmol) were dissolved in THF (20 mL). The solution was degassed, and NaH (0.0040 g, 0.17 mmol) was added. The mixture was then refluxed for 4 h. After cooling to RT, ice was added to the reaction mixture under vigorous stirring. The yellow precipitate generated was collected by vacuum filtration, washed with THF and water several times, and dried in the air. The resulting yellow powder was then redissolved in methylene chloride and washed with water three times. The methylene chloride layer was collected and dried over MgSO₄. The solvent was then removed under rotary evaporation. A yellow powder was collected after trituration with pentane. Yield: 0.050 g, 61%; ¹H NMR (CDCl₃): δ = 7.85 (s, 2H), 7.51–7.54 (m, 4H), 7.44 (d, J = 6.8 Hz, 4H), 7.29 (d, J = 16.0 Hz, 2H), 7.01 (d, J = 16.0 Hz, 2H), 1.52–2.07 ppm (m, 66H; 2(C₆H₁₁)₃); ³¹P{¹H} NMR (CDCl₃): δ = 57.6 ppm; HR-MS (ES⁺): m/z calcd: 1393.3512 [$M+H$]⁺; found: 1393.4550; UV/Vis (CH₂Cl₂): λ (ϵ) = 375 nm ($2.51 \times 10^4 \text{ M}^{-1} \text{ cm}^{-1}$); emission (CH₂Cl₂ ex. 375 nm): λ = 403, 429, 455 nm.

2,5-Bis(4-[(Cy₃P)Au]ethynylstyryl)-1,4-dibromobenzene (7): 1-[(Cy₃P)Au]-4-ethynylbenzene (0.1288 g, 0.212 mmol) and tetraethyl[(2,5-dibromo-1,4-phenylene)bis(methylene)]bis(phosphonate) (0.0683 g, 0.127 mmol) were dissolved in THF (20 mL). The solution was degassed, and NaH (0.0061 g, 0.255 mmol) was added. The mixture was then refluxed for 4 h. After cooling to RT, ice was added to the reaction mixture under vigorous stirring. The yellow precipitate generated was collected by vacuum filtration, washed with THF and water several times, and dried in the air. The dried powder was then redissolved in methylene chloride, and washed with water twice. The methylene chloride layer was collected and dried over MgSO₄. The solvent was then removed under rotary evaporation. A yellow powder was collected after trituration with pentane. Yield: 0.0837 g, 55%; ¹H NMR (CDCl₃): δ = 7.84 (s, 2H), 7.50 (d, J = 8.4 Hz, 4H), 7.42 (d, J = 8.4 Hz, 4H), 7.32 (d, J = 16.0 Hz, 2H), 7.00 (d, J = 16.4 Hz, 2H), 1.52–2.07 ppm (m, 66H; 2(C₆H₁₁)₃); ³¹P{¹H} NMR

(CDCl₃): δ = 56.9 ppm; HR-MS (ES⁺): m/z calcd: 1441.3512 [$M+H$]⁺; found: 1441.3093; elemental analysis calcd (%) for C₆₂H₈₀Au₂P₂Br₂: C 51.68, H 5.60; found: C 51.41, H 5.50; UV/Vis (CH₂Cl₂): λ (ϵ) = 279 (1.92 × 10⁴), 383 nm (4.03 × 10⁴ m⁻¹ cm⁻¹); emission (CH₂Cl₂ ex. 383 nm): λ = 421, 448 nm.

2,5-Bis(4-[(Cy₃P)Au]triazolostyryl)-1,4-dibromobenzene (8): 2,5-Bis(4-[(Cy₃P)Au]ethynylstyryl)-1,4-dibromobenzene (**7**) (0.0456 g, 0.032 mmol) was dissolved in dichloromethane (10 mL). Azidotrimethylsilane (0.0157 g, 0.13 mmol) and methanol (5 mL) were added to this solution. The resulting solution was degassed and stirred under Ar at RT vigorously. After stirring for about 10 min, the solution became turbid. This turbidity disappeared upon further stirring. After 48 h, solvents were removed under rotary evaporation, yielding a yellow residue, which was triturated to yield a yellow powder. Vapor diffusion of pentane into a saturated CHCl₃ solution gave an orange crystalline solid, which was collected, washed with pentane and dried under vacuum. Yield: 0.0341 g, 50%; ¹H NMR (CDCl₃): δ = 11.54 (brs, 2H), 8.37 (d, J = 8.4 Hz, 2H), 7.83–7.92 (m, 2H), 7.52–7.60 (m, 6H), 7.37 (d, J = 16.0 Hz, 8H), 7.10 (d, J = 16.0 Hz, 2H), 1.56–2.20 (m, 66H); ²(C₆H₁₁)₃; ³¹P{¹H} NMR (CDCl₃): δ = 58.5. MS (MALDI): m/z calcd: 1527.06 [M]⁺; found: 1527; elemental analysis calcd (%) for C₆₂H₈₂Au₂P₂Br₂N₆: C 48.77, H 5.41, N 5.50; found: C 49.03, H 5.15, N 5.24; UV/Vis (CH₂Cl₂): λ (ϵ) = 255 (2.41 × 10⁴), 260 (2.02 × 10⁴), 378 nm (3.07 × 10⁴ m⁻¹ cm⁻¹); emission (CH₂Cl₂ ex. 378 nm): λ = 462 nm.

2,6-Bis(4-[(Cy₃P)Au]styryl)naphthalene (9): 4-[(Cy₃P)Au]benzaldehyde (0.1235 g, 0.212 mmol) and tetraethyl[naphthalene-2,6-diylbis(methylene)]bis(phosphonate) (0.0540 g, 0.126 mmol) were dissolved in THF (20 mL). The solution was degassed, and NaH (0.0060 g, 0.252 mmol) was added. The mixture was then refluxed for 4 h. After cooling to RT, ice was added to the reaction mixture under vigorous stirring. The yellow precipitate generated was collected by vacuum filtration, washed with THF and water several times, and dried in the air. The resulting yellow powder was then redissolved in methylene chloride and washed with water three times. The methylene chloride layer was collected and dried over MgSO₄. The solvent was then removed under rotary evaporation. A yellow powder was collected after trituration with pentane. Diffusing pentane into a concentrated CHCl₃ solution yielded a powder, which was collected, washed with pentane and dried under vacuum. Yield: 0.040 g, 29%; ¹H NMR (CDCl₃): δ = 7.76 (d, J = 10.4 Hz, 4H), 7.71 (d, J = 9.6 Hz, 2H), 7.52–7.55 (m, 4H), 7.47 (d, J = 8.0 Hz, 4H), 7.19 (s, 4H), 1.56–2.07 ppm (m, 66H); ²(C₆H₁₁)₃; ³¹P{¹H} NMR (CDCl₃): δ = 57.8 ppm; HR-MS (ES⁺): m/z calcd: 1285.5457 [$M+H$]⁺; found: 1285.6199; elemental analysis calcd (%) for C₆₂H₈₄Au₂P₂: C 57.94, H 6.59; found: C 58.21, H 6.62; UV/Vis (CH₂Cl₂): λ (ϵ) = 291 nm (3.04 × 10⁴), 371 nm (6.00 × 10⁴ m⁻¹ cm⁻¹); emission (CH₂Cl₂ ex. 371 nm): λ = 400, 412 nm.

2,6-Bis(4-[(Cy₃P)Au]ethynylstyryl)naphthalene (10): 1-[(Cy₃P)Au]-4-ethynylbenzene (0.2030 g, 0.335 mmol) and tetraethyl[naphthalene-2,6-diylbis(methylene)]bis(phosphonate) (0.0792 g, 0.185 mmol) were dissolved in THF (20 mL). The solution was degassed, and NaH (0.0089 g, 0.370 mmol) was added. The mixture was then refluxed for 4 h. After cooling to RT, ice was added to the reaction mixture under vigorous stirring. The yellow precipitate generated was collected by vacuum filtration, washed with THF and water several times, and dried in the air. The dried powder was then redissolved in methylene chloride, and washed with water twice. The methylene chloride layer was collected and dried over MgSO₄. The solvent was then removed under rotary evaporation. A yellow powder was collected after trituration with pentane. Diffusing pentane into a concentrated CHCl₃ solution yielded a powder, which was collected, washed with pentane and dried under vacuum. Yield: 0.1032 g, 46%. ¹H NMR (CDCl₃): δ = 7.77–7.80 (m, 4H), 7.70 (d, J = 8.8 Hz, 2H), 7.49–7.52 (m, 4H), 7.43 (d, J = 8.4 Hz, 2H), 7.20 (d, J = 6.8 Hz, 2H), 1.50–2.03 ppm (m, 66H); ²(C₆H₁₁)₃; ³¹P{¹H} NMR (CDCl₃): δ = 56.9 ppm; HR-MS (FT-ICR): m/z calcd: 1333.54521 [$M+H$]⁺; found: 1333.54638; UV/Vis (CH₂Cl₂): λ (ϵ) = 279 (1.92 × 10⁴), 383 nm (4.03 × 10⁴ m⁻¹ cm⁻¹); emission (CH₂Cl₂ ex. 383 nm): λ = 421, 448 nm.

2,6-Bis(4-[(Cy₃P)Au]styryl)-1,5-dibromonaphthalene (11): 4-[(Cy₃P)Au]benzaldehyde (0.1879 g, 0.323 mmol) and tetraethyl[(4,8-dibromonaphthalene-2,6-diyl)bis(methylene)]bis(phosphonate) (0.1135 g,

0.194 mmol) were dissolved in THF (20 mL). The solution was degassed, and NaH (0.0093 g, 0.387 mmol) was added. The mixture was then refluxed for 4 h. After cooling to RT, ice was added to the reaction mixture under vigorous stirring. The yellow precipitate generated was collected by vacuum filtration, washed with THF and water several times, and dried in the air. The dried powder was then redissolved in methylene chloride, and washed with water twice. The methylene chloride layer was collected and dried over MgSO₄. The solvent was then removed under rotary evaporation. A yellow powder was collected after trituration with pentane. Diffusing pentane into a concentrated CHCl₃ solution yielded a powder, which was collected, washed with pentane and dried under vacuum. Yield: 0.1688 g, 72%; ¹H NMR (CDCl₃): δ = 8.30 (d, J = 8.8 Hz, 2H), 7.87 (d, J = 9.6 Hz, 2H), 7.71 (d, J = 16.0 Hz, 2H), 7.51–7.55 (m, 8H), 7.18 (d, J = 16.0 Hz, 2H), 1.58–2.17 ppm (m, 66H); ²(C₆H₁₁)₃; ³¹P{¹H} NMR (CDCl₃): δ = 57.8 ppm; HR-MS (FT-ICR): m/z calcd: 1443.36421 [$M+H$]⁺; found: 1443.36617; UV/Vis (CH₂Cl₂): λ (ϵ) = 245 (7.40 × 10³), 300 (6.12 × 10³), 380 nm (6.02 × 10³ m⁻¹ cm⁻¹); emission (CH₂Cl₂ ex. 380 nm): λ = 430, 454 nm.

2,6-Bis(4-[(Cy₃P)Au]ethynylstyryl)-1,5-dibromonaphthalene (12): 1-[(Cy₃P)Au]-4-ethynylbenzene (0.1538 g, 0.254 mmol) and tetraethyl[(4,8-dibromonaphthalene-2,6-diyl)bis(methylene)]bis(phosphonate) (0.0935 g, 0.159 mmol) were dissolved in THF (20 mL). The solution was degassed, and NaH (0.0077 g, 0.318 mmol) was added. The mixture was then refluxed for 4 h. After cooling to RT, ice was added to the reaction mixture while stirring. The yellow precipitate generated was collected by vacuum filtration, washed with THF and water several times, and dried in the air. The dried powder was then redissolved in methylene chloride, and washed with water twice. The methylene chloride layer was collected and dried over MgSO₄. The solvent was then removed under rotary evaporation. A yellow powder was collected after trituration with pentane. Diffusing pentane into a concentrated CHCl₃ solution yielded a powder, which was collected, washed with pentane and dried under vacuum. Yield: 0.0860 g, 47%; ¹H NMR (CDCl₃): δ = 8.33 (d, J = 9.2 Hz, 2H), 7.85 (d, J = 9.2 Hz, 2H), 7.74 (d, J = 16.0 Hz, 2H), 7.51 (dd, J = 15.2 Hz, 8.8 Hz, 8H), 7.15 (d, J = 16.0 Hz, 2H), 1.50–2.02 ppm (m, 66H); ²(C₆H₁₁)₃; ³¹P{¹H} NMR (CDCl₃): δ = 56.9 ppm; HR-MS (FT-ICR): m/z calcd: 1491.36522 [$M+H$]⁺; found: 1491.36621; elemental analysis calcd (%) for C₆₆H₈₂Au₂P₂Br₂: C 53.16, H 5.54; found: C 52.92, H 5.42; UV/Vis (CH₂Cl₂): λ (ϵ) = 315 nm (3.18 × 10⁴), 389 nm (4.53 × 10⁴ m⁻¹ cm⁻¹); emission (CH₂Cl₂ ex. 389 nm): λ = 415, 440 nm.

Calculations: Density-functional theory calculations were performed within Gaussian 09.^[56] Model compounds were chosen where cyclohexyl groups on phosphorus are replaced with methyls. Geometries were optimized in the gas phase without imposed symmetry, and harmonic frequency calculations indicated that converged structures were energy minima. Calculations employed the exchange and correlation functionals of Perdew, Burke, and Ernzerhof,^[57] and the TZVP basis set of Godbelt, Andzelm, and co-workers for carbon, hydrogen, and phosphorus.^[58] For gold, the Stuttgart 97 effective core potential and basis set were used.^[59] Hence, scalar relativistic effects are included implicitly. The calculations (including geometry optimizations) impose continuum solvation in chloroform, using the integral equation formalism of Tomasi's polarizable continuum model.^[49–52] Population analyses were performed with the AOMix software of Gorelsky.^[60,61]

Acknowledgements

The authors thank the U.S. National Science Foundation (grant CHE-1057659 to T.G.G.) for support. T.G.G. was an Alfred P. Sloan Foundation Fellow for 2009–2011. The diffractometer at Case Western Reserve was funded by NSF grant CHE-0541766; that at Youngstown State University, by NSF grant 0087210, by the Ohio Board of Regents grant CAP-491, and by Youngstown State University. N.D. thanks the government of Turkey for a fellowship.

- [1] E. L. Spitler, L. D. Shirtcliff, M. M. Haley, *J. Org. Chem.* **2007**, *72*, 86.
- [2] J. H. Burroughes, D. D. C. Bradley, A. R. Brown, R. N. Marks, K. Mackay, R. H. Friend, P. L. Burns, A. B. Holmes, *Nature* **1990**, *347*, 539.
- [3] J. R. Sheats, H. Antoniadis, M. Hueschen, W. Leonard, J. Miller, R. Moon, D. Roitman, A. Stocking, *Science* **1996**, *273*, 884.
- [4] M. Pawlicki, H. A. Collins, R. G. Denning, H. L. Anderson, *Angew. Chem.* **2009**, *121*, 3292; *Angew. Chem. Int. Ed.* **2009**, *48*, 3244.
- [5] Y. P. Yi, L. Y. Zhu, Z. G. Shuai, *Macromol. Theory Simul.* **2008**, *17*, 12.
- [6] A. D. Slepko, F. A. Hegmann, R. R. Tykwinski, K. Kamada, K. Ohta, J. A. Marsden, E. L. Spitler, J. J. Miller, M. M. Haley, *Opt. Lett.* **2006**, *31*, 3315.
- [7] Y. M. Sun, Y. W. Ma, Y. Q. Liu, Y. Y. Lin, Z. Y. Wang, Y. Wang, C. G. Di, K. Xiao, X. M. Chen, W. F. Qiu, B. Zhang, G. Yu, W. P. Hu, D. B. Zhu, *Adv. Funct. Mater.* **2006**, *16*, 426.
- [8] M. Elbing, G. C. Bazan, *Angew. Chem.* **2008**, *120*, 846; *Angew. Chem. Int. Ed.* **2008**, *47*, 834.
- [9] R. Schenk, H. Gregorius, K. Meerholz, J. Heinze, K. Müllen, *J. Am. Chem. Soc.* **1991**, *113*, 2634.
- [10] P. L. Burn, A. Kraft, D. R. Baigent, D. D. C. Bradley, A. R. Brown, R. H. Friend, R. W. Gymer, A. B. Holmes, R. W. Jackson, *J. Am. Chem. Soc.* **1993**, *115*, 10117.
- [11] T. Maddux, W. J. Li, L. P. Yu, *J. Am. Chem. Soc.* **1997**, *119*, 844.
- [12] A. Schmidt, M. L. Anderson, D. Dunphy, T. Wehrmeister, K. Müllen, N. R. Armstrong, *Adv. Mater.* **1995**, *7*, 722.
- [13] A. Kraft, A. C. Grimsdale, A. B. Holmes, *Angew. Chem.* **1998**, *110*, 416; *Angew. Chem. Int. Ed.* **1998**, *37*, 402.
- [14] R. E. Martin, F. Diederich, *Angew. Chem.* **1999**, *111*, 1440; *Angew. Chem. Int. Ed.* **1999**, *38*, 1350.
- [15] M. Strukelj, F. Papadimitrakopoulos, T. M. Miller, L. J. Rothberg, *Science* **1995**, *267*, 1969.
- [16] H. Meier, J. Gerold, H. Kolshorn, B. Mühling, *Chem. Eur. J.* **2004**, *10*, 360.
- [17] C. B. Nielsen, M. Johnsen, J. Arnbjerg, M. Pittelkow, S. P. McIlroy, P. R. Ogilby, M. Jorgensen, *J. Org. Chem.* **2005**, *70*, 7065.
- [18] J. F. Nierengarten, J. F. Eckert, J. F. Nicoud, L. Ouali, V. Krasnikov, G. Hadziioannou, *Chem. Commun.* **1999**, 617.
- [19] J. F. Eckert, J. F. Nicoud, J. F. Nierengarten, S. G. Liu, L. Echegoyen, F. Barigelletti, N. Armaroli, L. Ouali, V. Krasnikov, G. Hadziioannou, *J. Am. Chem. Soc.* **2000**, *122*, 7467.
- [20] N. Zhou, L. Wang, D. W. Thompson, Y. Zhao, *Tetrahedron Lett.* **2007**, *48*, 3563.
- [21] A. P. H. J. Schenning, A. C. Tsipis, S. C. J. Meskers, D. Beljonne, E. W. Meijer, J. L. Bredas, *Chem. Mater.* **2002**, *14*, 1362.
- [22] M. Fontana, H. Chanzy, W. R. Caseri, P. Smith, A. P. H. J. Schenning, E. W. Meijer, F. Gröhn, *Chem. Mater.* **2002**, *14*, 1730.
- [23] D. A. M. Egbe, C. P. Roll, E. Birckner, U. W. Grummt, R. Stockmann, E. Klemm, *Macromolecules* **2002**, *35*, 3825.
- [24] N. Zhou, L. Wang, D. W. Thompson, Y. Zhao, *Org. Lett.* **2008**, *10*, 3001.
- [25] C.-H. Zhao, A. Wakamiya, S. Yamaguchi, *Macromolecules* **2007**, *40*, 3898.
- [26] A. Wakamiya, K. Mori, S. Yamaguchi, *Angew. Chem.* **2007**, *119*, 4351; *Angew. Chem. Int. Ed.* **2007**, *46*, 4273.
- [27] H. Li, A. Sundararaman, K. Venkatasubbiah, F. Jäkle, *J. Am. Chem. Soc.* **2007**, *129*, 5792.
- [28] C.-H. Zhao, A. Wakamiya, Y. Inukai, S. Yamaguchi, *J. Am. Chem. Soc.* **2006**, *128*, 15934.
- [29] L. Gao, D. V. Partyka, J. B. Updegraff, N. Deligonul, T. G. Gray, *Eur. J. Inorg. Chem.* **2009**, 2711.
- [30] L. Gao, M. A. Peay, D. V. Partyka, J. B. Updegraff, T. S. Teets, A. J. Esswein, M. Zeller, A. D. Hunter, T. G. Gray, *Organometallics* **2009**, *28*, 5669.
- [31] D. V. Partyka, L. Gao, T. S. Teets, J. B. Updegraff, N. Deligonul, T. G. Gray, *Organometallics* **2009**, *28*, 6171.
- [32] D. V. Partyka, T. J. Robilotto, J. B. Updegraff, M. Zeller, A. D. Hunter, T. G. Gray, *Organometallics* **2009**, *28*, 795.
- [33] D. V. Partyka, T. J. Robilotto, M. Zeller, A. D. Hunter, T. G. Gray, *Proc. Natl. Acad. Sci. USA* **2008**, *105*, 14293.
- [34] D. V. Partyka, J. B. Updegraff, M. Zeller, A. D. Hunter, T. G. Gray, *Organometallics* **2007**, *26*, 183.
- [35] D. V. Partyka, M. Zeller, A. D. Hunter, T. G. Gray, *Angew. Chem.* **2006**, *118*, 8368; *Angew. Chem. Int. Ed.* **2006**, *45*, 8188.
- [36] M. Elian, M. M. L. Chen, D. M. P. Mingos, R. Hoffmann, *Inorg. Chem.* **1976**, *15*, 1148.
- [37] D. J. Gorin, F. D. Toste, *Nature* **2007**, *446*, 395.
- [38] J. S. Griffith, *Theory of Transition Metal Ions*, Cambridge University Press, Cambridge, pp. 437–439, **1964**.
- [39] M. A. Carvajal, J. J. Novoa, S. Alvarez, *J. Am. Chem. Soc.* **2004**, *126*, 1465.
- [40] W. Y. Heng, J. Hu, J. H. K. Yip, *Organometallics* **2007**, *26*, 6760.
- [41] T. Ishiyama, K. Ishida, N. Miyaura, *Tetrahedron* **2001**, *57*, 9813.
- [42] A. K. Bhattacharya, G. Thyagarajan, *Chem. Rev.* **1981**, *81*, 415.
- [43] R. Chincilla, C. Nájera, *Chem. Rev.* **2007**, *107*, 874.
- [44] M. Meldal, C. W. Tornøe, *Chem. Rev.* **2008**, *108*, 2952.
- [45] P. H. Gore, M. Yusuf, *J. Chem. Soc. C* **1971**, 2586.
- [46] M. A. Peay, J. E. Heckler, N. Deligonul, T. G. Gray, *Organometallics* **2011**, *30*, 5071.
- [47] J. Cornil, D. Beljonne, Z. Shuai, T. W. Hagler, I. Campbell, D. D. C. Bradley, J. L. Brédas, C. W. Spangler, K. Müllen, *Chem. Phys. Lett.* **1995**, *247*, 425.
- [48] F. Wu, W. Tian, J. Sun, J. Shen, X. Pan, Z. Shu, *Mater. Sci. Eng. B* **2001**, *85*, 165.
- [49] S. Miertuš, E. Scrocco, J. Tomasi, *Chem. Phys.* **1981**, *55*, 117.
- [50] J. Tomasi, B. Mennucci, R. Cammi, *Chem. Rev.* **2005**, *105*, 2999.
- [51] E. Cancès, B. Mennucci, J. Tomasi, *J. Chem. Phys.* **1997**, *107*, 3032.
- [52] B. Mennucci, E. Cancès, J. Tomasi, *J. Phys. Chem. B* **1997**, *101*, 10506.
- [53] R. S. Mulliken, *J. Chem. Phys.* **1955**, *23*, 1833.
- [54] F. G. Mann, A. F. Wells, D. Purdie, *J. Chem. Soc.* **1937**, 1828.
- [55] Bruker Advanced X-ray Solutions, SMART for WNT/2000 (Version 5.628), Bruker AXS Inc., Madison, Wisconsin: USA, 1997–2002.
- [56] Gaussian 09, M. J. Frisch, G. W. Trucks, H. B. Schlegel, G. E. Scuseria, M. A. Robb, J. R. Cheeseman, G. Scalmani, V. Barone, B. Mennucci, G. A. Petersson, H. Nakatsuji, M. Caricato, X. Li, H. P. Hratchian, A. F. Izmaylov, J. Bloino, G. Zheng, J. L. Sonnenberg, M. Hada, M. Ehara, K. Toyota, R. Fukuda, J. Hasegawa, M. Ishida, T. Nakajima, Y. Honda, O. Kitao, H. Nakai, T. Vreven, J. A. Montgomery, Jr., J. E. Peralta, F. Ogliaro, M. Bearpark, J. J. Heyd, E. Brothers, K. N. Kudin, V. N. Staroverov, R. Kobayashi, J. Normand, K. Raghavachari, A. Rendell, J. C. Burant, S. S. Iyengar, J. Tomasi, M. Cossi, N. Rega, J. M. Millam, M. Klene, J. E. Knox, J. B. Cross, V. Bakken, C. Adamo, J. Jaramillo, R. Gomperts, R. E. Stratmann, O. Yazyev, A. J. Austin, R. Cammi, C. Pomelli, J. W. Ochterski, R. L. Martin, K. Morokuma, V. G. Zakrzewski, G. A. Voth, P. Salvador, J. J. Dannenberg, S. Dapprich, A. D. Daniels, Ö. Farkas, J. B. Foresman, J. V. Ortiz, J. Cioslowski, D. J. Fox, Gaussian, Inc., Wallingford CT, **2009**.
- [57] J. P. Perdew, K. Burke, M. Ernzerhof, *Phys. Rev. Lett.* **1996**, *77*, 3865.
- [58] N. Godbout, D. R. Salahub, J. Andzelm, E. Wimmer, *Can. J. Chem.* **1992**, *70*, 560.
- [59] M. Dolg, U. Wedig, H. Stoll, H. Preuss, *J. Chem. Phys.* **1987**, *86*, 866.
- [60] S. I. Gorelsky, AOMix: Program for Molecular Orbital Analysis, York University, Toronto, **1997**. <http://www.sg-chem.net>.
- [61] S. I. Gorelsky, A. B. P. Lever, *J. Organomet. Chem.* **2001**, *635*, 187.

Received: August 11, 2011

Revised: January 5, 2012

Published online: March 30, 2012